Journal of Engineering Science and Technology
Vol. 17, No. 6 (2022) 4187 - 4202

ADSORPTION ISOTHERM ANALYSIS OF FLOATING COMPOSITE ZINC IMIDAZOLE FRAMEWORK-8 IN MILLIMETER EPOXY CUBES

ASEP BAYU DANI NANDIYANTO[1,*], SITI NUR HOFIFAH[2], RISTI RAGADHITA[1]

[1]Departemen Pendidikan Kimia, Universitas Pendidikan Indonesia, Jl. Dr. Setiabudhi No. 229, Bandung, Indonesia
[2]Departemen Pendidikan Biologi, Universitas Pendidikan Indonesia, Jl. Dr. Setiabudhi No. 229, Bandung, Indonesia
[*]Corresponding Author: nandiyanto@upi.edu

Abstract

This study evaluates the characteristics of composite zinc imidazole framework-8 (ZIF-8) in millimetre epoxy cubes in curcumin adsorption. In this study, ZIF-8 was mixed with resin and moulded into cubes. Curcumin was used as a model adsorbate. Adsorption was carried out by a batch experimental reactor at constant temperature and pH. The results were evaluated with several adsorption isotherm models Langmuir, Freundlich, Temkin, Dubinin-Raduskevich, Fowler-Guggenheim, Hill-Deboer, Jovanovic, Harkin-Jura, Flory-Huggins, Halsey. In addition to the evaluation of the adsorption isotherm, physical morphology characterization of the ZIF-8 cube was carried out using a digital microscope. The adsorption isotherm results showed that the adsorption process was suitable with the models of Jovanovic (R^2=0.9809), Hill-Deboer (R^2= 0.9344), Fowler-Guggenheim (R^2= 0.9238), Flory-Huggins (R^2= 0.8917), and Langmuir (R^2= 0.7081). The best fit model was the Jovanovic model. The adsorption process occurred with Chemisorption, monolayer, and spontaneous endothermic, and more than one zone of the active adsorbent was occupied by the adsorbate. This research is expected to become a new trend in the development of lightweight and floating adsorbents to increase the recyclability of adsorption.

Keywords: Adsorption isotherm, Curcumin, Composite, Metal-organic framework, Zinc imidazole framework.

1. Introduction

Zinc imidazole framework-8 (ZIF-8) belongs to the metal-organic framework (MOF) group which consists of metal ions and organic linkers/ligands. MOF materials have unique characteristics such as having high micropore volume, high crystallinity, and large pore size [1]. This unique surface characteristic is similar to the porous structure of activated carbon and zeolite. MOF materials are one of the popular materials [2].

Recently, ZIF-8 has been studied and developed in wastewater treatment as an absorbent material. ZIF-8 can be used as an adsorbent because it maintains very high chemical stability in aqueous environments. ZIF-8 also has good adsorption capacity. Therefore, ZIF-8 is widely used in wastewater treatment and is suitable to absorb pollutants in water, dyes, and dissolved chemical materials. Several studies on the use of ZIF-8 for adsorption have been carried out. ZIF-8 was used to remove Cr (IV) from water [3], antibiotics [4], tetracycline from an aqueous solution [5], radioactive iodine [6], heavy metals from the solution [7], congo red [8], and many more studies on adsorption using ZIF-8. The unique properties of ZIF-8 give it a superior adsorption capacity. However, ZIF-8 particles tend to clump together and result in a decrease in the specific surface area [9] They also have weak recyclability, as it is difficult to separate them from the water after removing pollutants [10, 11]

Our previous studies have reported how to prepare various MOF materials ((i.e. MIL-100(Fe), HKUST-1(Cu), Cu-TPA, and MOF-5(Zn))) [12, 13] as well as ZIF-8 [14] particles with controllable sizes from nano to micrometres. The synthesis was also supported by the adsorption process [15]. We also explained the feasibility study for the production of MOF particles [16]. Here, we made ZIF-8 which is lightweight and floats in solution. We mixed ZIF 8 particles with resin and moulded them into cubes. The moulded process creates ZIF-8 floatable, making it easy to recycle after use.

This study aimed to evaluate the isotherm adsorption ability of the ZIF-8 millimetre cube. Ten adsorption isotherm models were used to characterize the suitable adsorption models. This analysis was supported by a UV-Vis spectrophotometer. UV-Vis is used to read the concentration of the solution. The result was interpreted using the isotherm adsorption model equation. We also performed surface morphology characterization of ZIF-8 using a digital microscope. This research is expected to become a new trend in the development of lightweight and floating adsorbents.

2. Isotherm Adsorption Models

Ten adsorption isotherm models, including Langmuir, Freundlich, Temkin, Dubinin-Radushkevich, Fowler-Guggenheim, Hill-Deboer, Jovanovic, Harkin-Jura, Flory-Huggins, and Halsey, were used to assess the phenomenon during the adsorption process. When adsorption takes place in a monolayer, multilayer, or cooperative fashion, it may be a phenomenon of common adsorption processes. Figure 1 illustrates the phenomenon of the monolayer, multilayer, and cooperative adsorption processes.

For adsorption analysis, several parameters are required. Table 1 shows the adsorption isotherm equations used in this study, and Table 2 shows some of the

parameters evaluated in this study. To clarify, an explanation of the adsorption isotherm is described in further detail.

The adsorption process is defined by the Langmuir isotherm for both monolayer and multilayer formatting. Whether adsorption is a physical or chemical process depends on it. The Langmuir isotherm is based on four assumptions: (1) each site can only adsorb one adsorbate molecule; (2) each fixed site can only adsorb one molecule; (3) all sites have the same energy; and (4) there is no interaction between the adsorbed molecules and the nearby sites. Langmuir model is represented in eq. (1) (see Table 1).

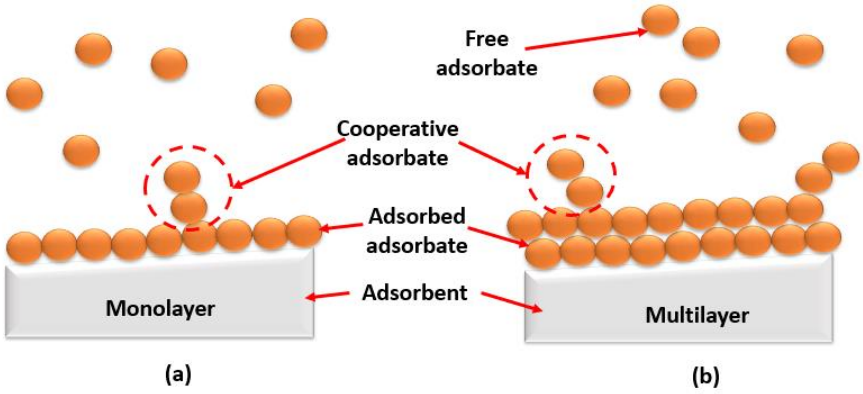

Fig. 1. Detailed illustration of adsorption phenomena.

The separation factor (R_L), which is described in Eq. (2) (see Table 2), is a dimensionless factor present in the Langmuir isotherm. R_L parameters are used to support the adsorption process because they are crucial for analysing each adsorption case to determine whether it is favourable or unfavourable. The R_L value decreasing, indicating the adsorption process, is desired. The R_L essentially forecasts the affinity between the adsorbent and adsorbate. R_L parameters are described as follows: (i) $R_L > 1$ describes unfavourable adsorption because desorption occurs, (ii) $R_L = 1$ explains a linear adsorption process that does not depend on the concentration, and (iii) $R_L = 0$ describes irreversible adsorption process because the adsorbate cannot diffuse (usually occurs in chemisorption).

The Freundlich isotherm is based on the adsorption process that takes place on heterogeneous surfaces to create multilayers. Interactions between adsorbed molecules are possible with multilayer adsorption. As a result, this model suggests that the energy is not constant across all surface sites [17]. Eq. (3) (see Table 1) can be used to represent Freundlich's isotherm model. In eq. (3), there are n and $1/n$ parameters that describe as follows: (i) $n < 1$ explains the chemisorption process's characteristics, (ii) $n = 1$ explains a linear adsorption process where the partition between two phases is independent of concentration, (iii) $n > 1$ explains the physisorption process's characteristics, (iv) $1/n < 1$ explains the normal adsorption process, (v) $1/n > 1$ explains the cooperative adsorption process, and (vi) $0 < 1/n < 1$ explains the favourable adsorption process due to the lack of a desorption process.

When using extremely low adsorbate concentrations, the Temkin isotherm describes the indirect adsorbate interaction [17]. The heat of adsorption for each molecule in the multilayer is calculated using eq. (4) (see Table 1). The definition of β_T is described as follows: (i) β_T < 8 kJ/mol explains the characteristics of physical adsorption, and (ii) β_T > 8 kJ/mol explains The characteristics of chemical adsorption.

The Dubinin-Raduskevich isotherm assumes that adsorption takes place on heterogeneous surfaces. Eq. (5) displays the Dubinin-Radushkevich model's adsorption equation (see Table 1). The Dubinin-Radushkevich isotherm constant correlated with the average free adsorption energy per mole of adsorbate [17]. Eq. (6) in Table 1 express the Polanyi potential and calculate the adsorption energy and Eq. (7) in Table 2 express the free energy of adsorption for each adsorbate molecule. *E* parameter is described as follows: (i) E < 8 kJ/mol explains the process occurring are physical adsorption, and (ii) E > 8 kJ/mol explains the process occurring are chemical adsorption.

The Fowler-Guggenheim isotherm explains the lateral interactions between the adsorbed molecules [17]. Eq. (8) in Table 1 shows the Fowler-Guggenheim isotherm equation. In the Fowler-Guggenheim isotherm equation, there is a W parameter that is described as follows: (i) W > 0 kJ/mol explains the process has an exothermic attractive force between the adsorbed molecules, (ii) W < 0 kJ/mol explains the adsorbed molecules and the process repel one another in an endothermic way, and (iii) W = 0 kJ /mol explains adsorbed molecules do not interact with one another.

The Hill-de Boer isotherm explains mobile adsorption as well as the existence of lateral interactions between the molecules that have been adsorbed [17]. Eq. (9) in Table 1 represents the equation for the Hill-de Boer isotherm. In the Hill-de Boer parameter, there is a K_2 parameter that is described as follows: (i) K_2 > 0 kJ/mol explains the attractive force between the adsorbed molecules and the process is exothermic, (ii) K_2 < 0 kJ/mol explains the adsorbed molecules and the process repel one another in an endothermic way, and (iii) K_2 = 0 kJ/mol explains adsorbed molecules do not interact with one another.

The Jovanovic isotherm is based on the Langmuir model phenomena, it forbids mechanical contact between the adsorbent and adsorbate [17]. Eq. (10) in Table 1 illustrates the linear equation of the Jovanovic isotherm.

The adsorption that takes place on a heterogeneous surface is measured by the Harkin-Jura isotherm. A multilayer is created during the adsorption process [17]. Eq. (11) in Table 1 represents the equation of this model.

The Flory-Huggins isotherm assumes that the adsorption process happens spontaneously and accounts for the surface coverage of the adsorbate on the adsorbent [17]. The Flory-Huggins isotherm is shown in eq. (12) (see Table 1). The Gibbs free energy of Flory-Huggins isotherm can be calculated by eq. (13) (see Table 1).

The Halsey isotherm measures the multilayer characteristics of adsorption [17]. Eq. (14) in Table 1 clearly shows the Halsey isotherm's equation. Additionally, the amount adsorbed by the unit mass of the adsorbent at equilibrium (*Qe*) is calculated using eq. (15) (see Table 1).

Table 1. Isotherm adsorption equation used

Adsorption Isotherm Model	Equation	Equation number
Langmuir	$\frac{1}{Q_e} = \frac{1}{Q_{max} K_L} \frac{1}{C_e} + \frac{1}{Q_{max}}$	(1)
	$R_L = \frac{1}{1 + K_L C_e}$	(2)
Freundlich	$\log Q_e = log k_f + \frac{1}{n} \log C_e$	(3)
Temkin	$q_e = B_T ln A_T + B_T ln C_e$	(4)
Dubinin-Raduskevich	$lnq_e = lnq_s - (\beta \varepsilon^2)$	(5)
	$\varepsilon = RTln\left[1 + \frac{1}{C_e}\right]$	(6)
	$E = \frac{1}{\sqrt{2\beta}}$	(7)
Fowler-Guggenheim	$K_{FG} C_e = \frac{\theta}{1-\theta} \exp\left(\frac{2.\theta.W}{RT}\right)$	(8)
Hill-de Boer	$K_1 . C_e = \frac{\theta}{1-\theta} \exp\left(\frac{\theta}{1-\theta} - \frac{K_2 \theta}{RT}\right)$	(9)
Jovanovic	$lnQ_e = lnQ_{max} - K_J C_e$	(10)
Harkin-Jura	$\frac{1}{q_e^2} = \frac{B_{HJ}}{A_{HJ}} - \left(\frac{1}{A}\right) log C_e$	(11)
Flory-Huggins	$log \frac{\theta}{C_e} = log K_{FH} + n \log(1-\theta)$	(12)
	$\Delta G° = -RTlnK_{FH}$	(13)
Halsey	$Q_e = \frac{1}{n_H} lnK_H - \left(\frac{1}{n_H}\right) lnC_e$	(14)
	$Q_e = \frac{C_o - C_e}{m} \times V$	(15)

Table 2. Parameter used in the adsorption analysis.

No.	Symbol	Unit	Note	Isotherm model
1	Q_e	mg/g	the number of adsorbed adsorbate molecules per gram of adsorbent	Langmuir
2	Q_{max}	mg/g	the capacity of the adsorbent monolayer	Langmuir
3	K_L		the Langmuir adsorption constant relating to the adsorption energy	Langmuir
4	C_e	mg/L	the adsorbate equilibrium concentration	Langmuir, Freundlich
5	K_f		the relative adsorption capacity	Freundlich
6	n		the degree of non-linearity	Freundlich
7	$1/n$		the adsorption strength	Freundlich
8	A_T		the Temkin isotherm model's equilibrium constant	Temkin
9	β_T		the model's Temkin isotherm	Temkin
10	qs	mg/g	the hypothetical saturation capacity	Dubinin-Raduskevich
11	ε		the Polanyi potential related to equilibrium conditions	Dubinin-Raduskevich
12	β		the Dubinin-Radushkevich isotherm constant	Dubinin-Raduskevich
13	K_{FG}	L/mg	the Fowler-Guggenheim equilibrium constant	Fowler-Guggenheim
14	W	kJ/mol	the energy of interaction	Fowler-Guggenheim
15	K_1	L/mg	the Hill-de Boer constant	Hill-de Boer
16	K_2	L/mg	the energetic constant of the adsorbed molecular interaction	Hill-de Boer
17	K_J		the Jovanovic constant	Jovanovic
18	B_{HJ}		the adsorbent's specific surface area	Harkin-Jura
19	A_{HJ}		the Harkin-Jura isotherm constant	Harkin-Jura
20	K_{FH}		the constant of Flory-Huggins	Flory-Huggins
21	n_{FH}		the quantity of adsorbate that is occupying the adsorption site	Flory-Huggins
22	ΔG°		The Gibbs free energy of adsorption	Flory-Huggins
23	K_H		the constants of Halsey's	Halsey
24	C_o	mg/L	the initial concentration	Halsey
25	m	g	is the adsorbent mass	Halsey
26	V	L	the adsorbate solution volume	Halsey

3. Methods

3.1. Materials

Several chemicals are used to synthesize ZIF-8 including Zinc nitrate ($Zn(NO_3)_2.6H_2O$), and precursor 2-Methyl Imidazole (MIM). In this study, methanol was used as a solvent. As the model adsorbate, we used a coloured solution obtained from dissolved powdered curcumin.

3.2. ZIF-8 particles production

ZIF-8 particles were produced in this study using an aqueous synthesis method. Detailed information for the synthesis of ZIF-8 is explained in our previous study [15]. In a different container, a methanol solution was used to dissolve zinc nitrate and 2-MIM precursors with the right composition. Two precursors were combined to create a dissolved solution mixture after each precursor in the various containers had been completely dissolved in methanol. The combination, which was initially an uncoloured mixture of solutions, was then agitated for the following eight hours at room temperature. The solution turns white as a result of the solid suspension of ZIF-8 particles that develops. The ZIF-8 particles were successfully created at this point. To separate the filtrate and ZIF-8 particles, the combination of the solution was centrifuged and filtered. The remaining methanol solvent was then removed from the collected ZIF-8 particles by drying them in an oven at below 50°C for an hour. Figure 2 shows an illustration of the ZIF-8 particle production [18].

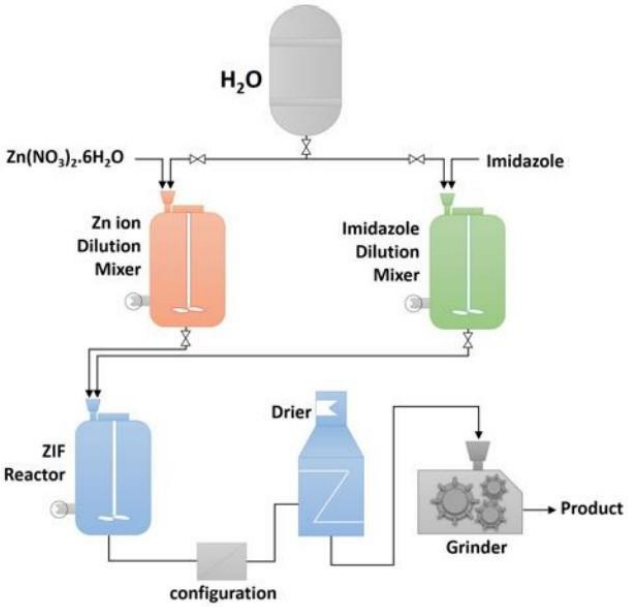

Fig. 2. Illustration of ZIF-8 production (adapted from reference [15]).

3.3. ZIF-8 cube production

Cube adsorbent was made by mixing ZIF-8 particles and resin material. The type of resin used here was Bisphenol A-epichlorohydrin and cyclo aliphatic amine. ZIF-8 particles and resin materials were mixed in a ratio of 1:6. To make 3.5 g

of cube adsorbent, 0.5 g of ZIF-8 was mixed into 3 g of the resin mixture. After that, the mixture was moulded using a silicon mold with dimensions of 1 x 1 x 1 cm. The mixture was then dried at room temperature for 14 days. In addition to evaluating the adsorption isotherm model that is suitable for the adsorption phenomenon occurs, we also analysed the morphological characteristics of the ZIF-8 Cube before and after the adsorption process. A digital microscope was used in this characterization. Detailed preparation of composite in resin is reported in our previous studies [19-27].

3.4. Adsorption process method

Batch isotherm adsorption experiments were conducted in 500 mL of borosilicate glass. Before use, the ZIF-8 cube was scraped off. Scraping is done to remove the resin on the surface of the cube and make ZIF-8 particles exposed and get direct contact with the adsorbate. The process of adsorption involves adding a 0.19 g of ZIF-8 cube as an adsorbent to 150 mL of curcumin solutions of a specific concentration (i.e., 20, 40, 60, 80, and 100 ppm) and stirring at 1000 rpm for 1.5 hours at a constant pH, temperature, and pressure. We selected a rotation speed of 1000 rpm to avoid desorption or poor interaction between adsorbate-adsorbent.

Turmeric powder (Curcuma Longa; Desaku, local turmeric powder, Bandung, Indonesia) was used to create a curcumin solution. The curcumin solution was chosen as an adsorbate model for safety reasons and because curcumin has the ideal molecular size for an organic molecule. Before being analysed, the curcumin solution was centrifuged and filtered to separate the filtrate material from the curcumin solution. The absorbance of the curcumin solution was then determined using a UV-VIS spectrophotometer (Model 705; JENWAY; Cole-Parner; US) operating at a wavelength of 250–500 nm. Detailed information for the UV-Vis spectrophotometer analysis is explained in our previous report [28].

Based on the Lambert-Beer analysis, the absorbance of the curcumin solution was plotted, normalized, and calculated. The UV-Vis was utilized to understand concentration, and literature was employed to read and interpret the results [28]. Then, as detailed in reference [17], data from UV-vis was computed using standard isotherm adsorption. The acquired data were then plotted and contrasted with the Langmuir, Freundlich, Temkin, Dubinin-Radushkevich, Fowler-Guggenheim, Hill-Deboer, Jovanovic, Harkin-Jura, Flory-Huggins, and Halsey.

4. Results and Discussion

ZIF-8 lightweight adsorbent showed good performance during the experiment. When the ZIF-8 cube is put into the curcumin solution, this lightweight adsorbent float on the surface of the solution. After the batch adsorption was complete, the ZIF-8 cube changes to a yellow colour and sinks to the bottom of the glass. This indicates the success of the adsorption process. The large number of curcumin particles absorbed makes the ZIF-8 a lightweight cube. However, packaging ZIF-8 into cubes made it easier for ZIF-8 to be removed from the solution and recycled for reuse for the next adsorption batch. Figure 3 shows the results of surface characterization of the ZIF-8 cube based on analysis using a digital microscope. Figure 3(a) shows the surface morphology of ZIF-8 before adsorption. It appears

that the ZIF-8 cube is still white and clean. Figure 3(b) shows the surface morphology of the ZIF-8 cube after adsorption. The surface of the ZIF-8 cube turns orange as it absorbs the colour from the curcumin solution. The surface of the cube was not smooth because of the scraped-off done. The scraped-off exposes the resin-bound ZIF-8 particles to increase the adsorption capacity. Scraped off also makes the pores on the cube open so that the surface area of the adsorbent increases. ZIF-8 has a large pore hierarchy (0.69 cm^3/g). Two different pore regimes are present in ZIF-8 (micropore-mesopore, or mesopore–macropore) [28]. These characteristics make a lightweight ZIF-8 adsorbent have a good performance in adsorption, even though it has been packaged into a cube.

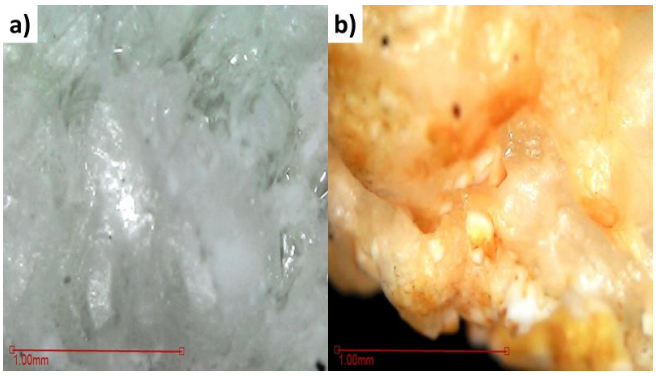

Fig. 3. (a) The surface of ZIF-8 cube before adsorption, (b) The surface of ZIF-8 cube after adsorption.

The results of the linearization of the Langmuir, Freundlich, Temkin, Dubinin-Radushkevich, Fowler-Guggenheim, Hill-Deboer, Jovanovic, Harkin-Jura, Flory-Huggins, and Halsey adsorption models are shown in Figs. 4 (a)-(j). A more detailed description of the ten model adsorption characterization is shown in Table 3.

Figure 4(a) is the linearization curve of the Langmuir isotherm adsorption model. The adsorption process fits the Langmuir isotherm model because R^2>0.7. Based on Table 3, the adsorption phenomenon that occurs is Favourable and monolayer adsorption. The adsorption process takes place chemically by forming bonds between curcumin particles and ZIF-8 particles [29]. Thus, the chemical bond along the surface of the lightweight adsorbent cube forms a monolayer.

Figure 4(b) shows the curve of the Freundlich isotherm model. Based on the R^2 value, the Freundlich adsorption model is not suitable for explaining the adsorption process. Parameter 1/*n* indicates the adsorption process occurs normally. While the *n* parameter indicates the adsorption process that occurs is adsorption with chemical interactions [30]. ZIF-8 is a particle that easily interacts chemically with other compounds. ZIF-8 is even reported to be able to form strong chemical bonds with cellulose-based nanomaterials [31].

Figure 4(c) shows the yield curve of the Temkin isotherm adsorption. Based on the results of linearization, the Temkin isotherm model was not suitable for the adsorption process (R^2<0.7). The linearity value describes the distribution of the adsorbate on the surface of the adsorbent that is not uniform [32]. In addition, the B_T parameter from Table 3 shows that the adsorption isotherm occurs through physical interactions (B_T <8 kJ/mol).

Table 3. Adsorption characteristics based on standard isotherm models.

Isotherm Model	Parameters	Value	Note
Langmuir	q_m (mg/g)	1.2832	Maximum adsorption capacity
	K_L (L/mg)	-0.0932	Maximum adsorption capacity
	R^2	0.7081	Favourable and monolayer adsorption ($R^2 > 0.70$)
Freundlich	K_f (mg/g)	0.5807	Capacity of adsorption
	$1/n$	-0.5436	Normal adsorption
	n	-1.8396	Chemisorption (n < 1)
	R^2	0.6365	Coefficient of correlation
Temkin	B_T (kJ/mol)	-16.3576	Physical adsorption (βT < 8 kJ/mol)
	A_T (L/mg)	2.9174×10^{42}	Equilibrium binding constant
	R^2	0.6941	Non-uniform adsorbate distribution on the adsorbent surface ($R^2 < 0.70$)
Dubinin-Radushkevich	β	8.5787	Dubinin-Radushkevich Constant
	qs (mg/g)	1.0271	Capacity of adsorption
	E (kJ/mol)	0.2414	E < 8 kJ/mol indicates physical adsorption
	R^2	0.6242	On the surface of the adsorbent, no micropores ($R_2 < 0.70$)
Fowler-Guggenheim	K_{FG} (L/mg)	1.8518×10^{-8}	The Constanta of Fowler-Guggenheim
	W (kJ/mol)	-17.947	Endothermic adsorption process
	R^2	0.9238	Multilayer adsorption ($R^2 > 0.70$)
Hill-Deboer	K_1 (L/mg)	2.5412×10^{-4}	Hill-Deboer constant
	K_2 (kJ/mol)	-498.9555	Endothermic adsorption process
	R^2	0.9344	Multilayer adsorption ($R^2 > 0.70$)
Jovanovic	K_j (L/g)	0.3105	Jovanovic constant
	q_m (mg/g)	0.8632	Maximum adsorption capacity
	R^2	0.9809	Monolayer adsorption on the surface of adsorbent ($R^2 > 0.70$)
Harkin-Jura	A_H (g^2/L)	0.6019	Harkin-Jura constant
	B_H (mg^2/L)	-1.2826	Surface area of the adsorbent
	R^2	0.5546	Monolayer adsorption ($R_2 < 0.70$)
Flory Huggins	K_{FH} (L/g)	1.7486	Flory Huggins equilibrium constant
	n_{FH}	-0.671	More than one active adsorbent zone ($n_{FH} < 1$)
	R^2	0.8917	Multilayer adsorption on the surface of adsorbent ($R^2 > 0.70$)
Halsey	n_H (L/mg)	-1.8396	Halsey constant
	K_H	15.9251	Halsey constant
	R^2	0.6365	Monolayer on the surface of the adsorbent ($R^2 > 0.80$)

Figure 4(d) shows the linearization curve of the Dubinin-Raduskevich isotherm adsorption model. The adsorption process is not suitable for this isotherm model because R^2<0.7. Table 3 shows the parameter E less than 8 kJ/mol. This confirms that the adsorption process occurs physically [33] But, the low R^2 value confirms that physisorption may only occur in some areas of the adsorbent. Physical adsorption has a low tensile strength, and the energy required for the process does not exceed 8 kJ/mol, allowing the adsorbate to move to the other side of the adsorbent or even be released back into the solution [34].

Figure 4(e) shows the linearization of the Fowler-Guggenheim isotherm model. The adsorption process is following this adsorption model. R^2>0.7 confirms that adsorption occurs to form a multilayer. Table 3 confirms that the adsorption process also occurs endothermic. Meanwhile, the same result was shown by the Hill-Deboer adsorption model. Figure 4(f) shows the results of plotting the Hill-Deboer isotherm adsorption model. The adsorption phenomenon fits with this isotherm model. The Hill-Deboer model also confirms that the attractive force between the adsorbate and adsorbent occurs through endothermic interactions [35]. Several studies also reported that ZIF-8 adsorbed adsorbates such as congo red or even mixed pollutants with spontaneous endothermic adsorption. [8, 36].

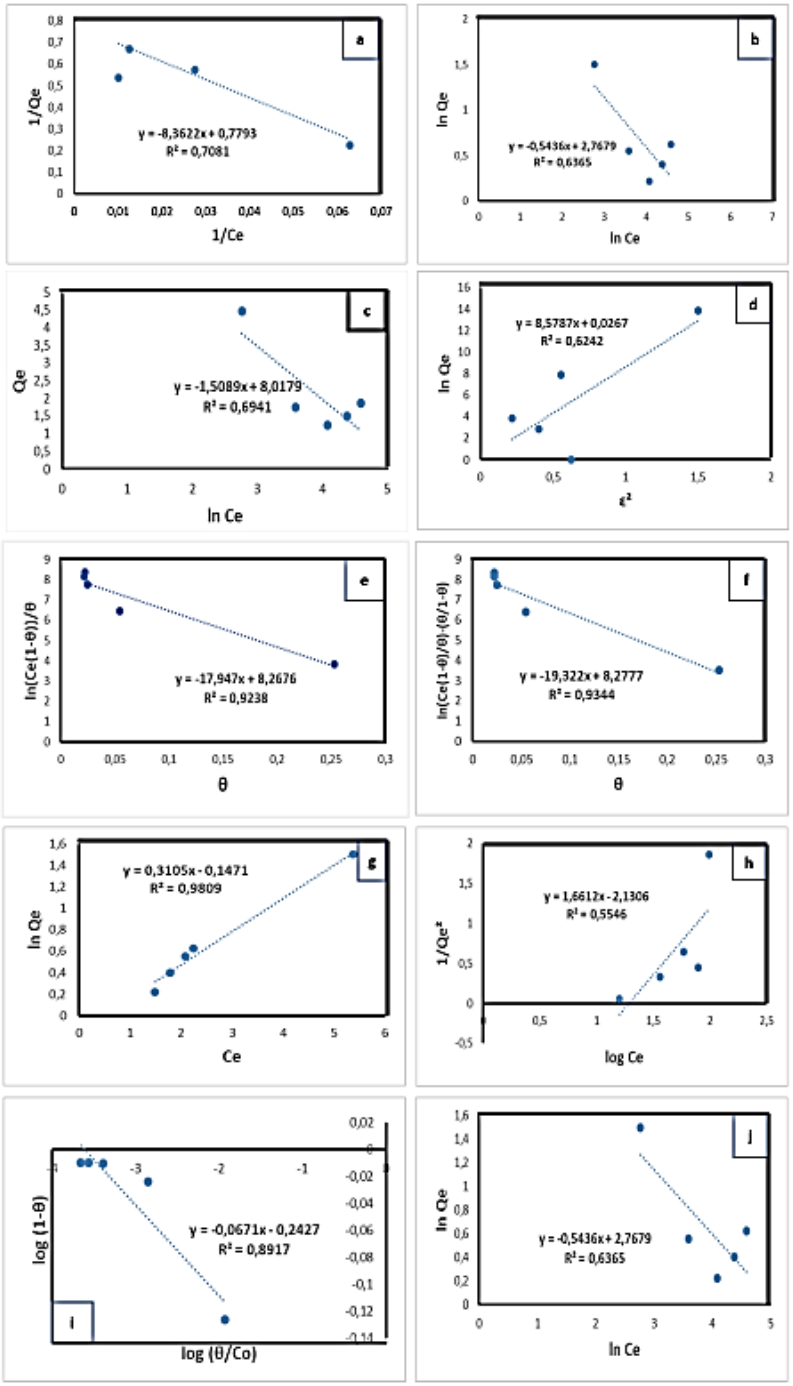

Fig. 4. The Isotherm adsorption (a) Langmuir, (b) Freundlich, (c) Temkin, (d) Dubinin-Radushkevich, (e) Fowler-Guggenheim, (f) Hill-Deboer, (g) Jovanovic, (h) Harkin-Jura, (i) Flory-Huggins, and (j) Halsey

Figure 4(g) is the curve result of the installation of the Jovanovic isotherm adsorption. The Jovanovic model is most suitable to explain the adsorption phenomenon that occurs (the R^2 value is closest to 1). Jovanovic's model assumes the same thing as Langmuir's model. Following Langmuir's model, this adsorption model also explains that adsorption occurs in a monolayer manner. The Jovanovic isotherm model showed a maximum adsorption capacity (Q_{max}) of 0.8632 mg/g while the Langmuir isotherm model showed a larger capacity of 1.2832 mg/g. Both of these models strengthen the explanation that on most of the adsorbent sides occurs adsorption that forms a monolayer. The monolayer adsorption process informs that the adsorbate is evenly distributed over the entire surface of the adsorbent [37]. Monolayer adsorption also describes adsorption that occurs without any lateral interactions [38].

The results of the linearization of Harkin Jura's isotherm adsorption model are shown in Fig. 4(h). Based on the R^2 value, the Harkin-Jura model is not suitable to explain the adsorption process. However, this R^2 confirms the result that adsorption occurs in a monolayer manner. A_H and B_H parameter values based on calculations were 0.6019 g^2/L and -1.2826 mg^2/L, respectively.

Figure 4(i) shows the results of the fitting data of Flory Huggins' isotherm adsorption model. The value of R^2 indicates that the adsorption process is following this isotherm model. Table 3 shows the n_{FH} value of less than 1, it explains that more than one zone of the active adsorbent was occupied by the adsorbate. The adsorption process also forms a multilayer. Flory Huggins' also assumed that the adsorption process occurred spontaneously [39].

Figure 4(j) shows the results of fitting Halsey's isotherm adsorption model data. Halsey's isotherm model is not suitable to explain the adsorption phenomenon in this experiment ($R^2 < 0.7$). Based on the calculation results of the Halsey isotherm model, the nH and KH parameters are -1.8396 (L/mg) and 15.9251 (see Table 3), respectively. Although the Halsey model does not suitable for the adsorption phenomenon, this isotherm model also confirms that the adsorption process occurs in a monolayer.

The overall adsorption process that occurs is depicted in Fig. 5. The adsorption isotherm models that are most suitable to explain the phenomena that occur in this experiment are Jovanovic, Hill-Deboer, Fowler-Guggenheim, Flory-Huggins, and Langmuir. The five adsorption isotherm models explain that in this experiment, adsorption occurs in a monolayer, spontaneously endothermic adsorption, chemisorption, and more than one zone of the active adsorbent was occupied by the adsorbate.

Several other isotherm models strengthen the assumption of the phenomenon that occurs. Freundlich's isotherm adsorption model supports the assumption that the adsorption process occurs by chemisorption. The Harkin-Jura and Halsey isotherm adsorption model supports the assumption of a monolayer adsorption process. Meanwhile, other adsorption isotherm models explain different phenomena that occur on some sides of the adsorbent. The adsorption model of Temkin and Dubinin-Radushkevich, explains that on some sides of the adsorbent physical adsorption interactions occur. Flory Huggins' isotherm adsorption model also assumes in some side of the adsorbent occurred multilayer adsorption. This phenomenon could happen because some sides of the adsorbent may have different

energies so the adsorption process can occur physically or chemically, by forming monolayers, or multilayers [40].

The above data is in good agreement with our previous studies [15, 41-46], confirming the effectiveness of the present analysis of adsorption to explore and visualize the phenomena during the adsorption and giving ideas for further research to be done.

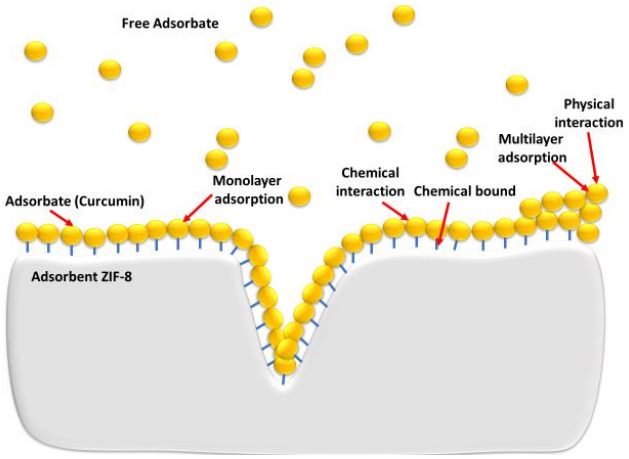

Fig. 5. The illustration of the overall adsorption phenomenon that occurs in this experiment.

5. Conclusion

This study investigated the characteristics of zinc imidazole framework-8 (ZIF-8) lightweight to adsorb the curcumin solution. This research used several adsorption isotherm models: Langmuir, Freundlich, Temkin, Dubinin Raduskevich, Fowler-Guggenheim, Hill-Deboer, Jovanovic, Harkin-Jura, Flory-Huggins, Halsey to evaluate the phenomenon that occurred when the adsorption process. The results of the adsorption isotherm show that the best fit adsorption model in this experiment is Jovanovic (R^2= 0.9809), Hill-Deboer (R^2= 0.9344), Fowler-Guggenheim (R^2= 0.9238), Flory-Huggins (R^2= 0.8917), and Langmuir (R^2= 0.7081). There most suitable adsorption model describes the adsorption process that occurred with chemisorption, monolayer, spontaneous endothermic, and more than one zone of the active adsorbent was occupied by the adsorbate. However, Freundlich, Harkin-Jura, and Halsey's isotherm adsorption model strengthen the assumption that the adsorption process occurs by chemisorption and monolayer. Meanwhile, the Temkin and Dubinin-Radushkevich model explains another phenomenon, the adsorption process also occurs in a multilayer manner on some sides of the adsorbent. This research is expected to provide new information about the development of lightweight adsorbents.

References

1. Delaporte, N.; Rivard, E.; Natarajan, S.K.; Benard, P.; Trudeau, M.L.; and Zaghib, K. (2020). Synthesis and performance of MOF-based non-noble metal catalysts for the oxygen reduction reaction in proton-exchange membrane fuel cells: a review. *Nanomaterials*, 10(10), 1-61.

2. Shidiq, A.P.A. (2023). Bibliometric analysis of nano metal-organic frameworks synthesis research in medical science using VOSviewer. *ASEAN Journal of Science and Engineering*, 3(1), 31-38.
3. Bo, S.; Ren, W.; Lei, C.; Xie, Y.; Cai, Y.; Wang, S.; and Yao, J. (2018). Flexible and porous cellulose aerogels/zeolitic imidazolate framework (ZIF-8) hybrids for adsorption removal of Cr (IV) from water. *Journal of Solid State Chemistry*, 262(2018), 135-141.
4. Chen, X.; Jiang, X.; Yin, C.; Zhang, B.; and Zhang, Q. (2019). Facile fabrication of hierarchical porous ZIF-8 for enhanced adsorption of antibiotics. *Journal of Hazardous Materials*, 367(2019), 194-204.
5. Sun, S.; Yang, Z.; Cao, J.; Wang, Y.; and Xiong, W. (2020). Copper-doped ZIF-8 with high adsorption performance for removal of tetracycline from aqueous solution. *Journal of Solid State Chemistry*, 285(2020), 1-9.
6. Lee, Y.R.; Do, X.H.; Cho, K.Y.; Jeong, K.; and Baek, K.Y. (2020). Amine-functionalized zeolitic imidazolate framework-8 (ZIF-8) nanocrystals for adsorption of radioactive iodine. *ACS Applied Nano Materials*, 3(10), 9852-9861.
7. Li, K.; Miwornunyuie, N.; Chen, L.; Jingyu, H.; Amaniampong, P.S.; Ato Koomson, D.; and Lu, H. (2021). Sustainable application of ZIF-8 for heavy-metal removal in aqueous solutions. *Sustainability*, 13(2), 1-11.
8. Cao, X.Q.; Wang, X.; Chen, M.; Xiao, F.; Huang, Y.M.; and Lyu, X.J. (2021). Synthesis of nanoscale zeolitic imidazolate framework-8 (ZIF-8) using reverse micro-emulsion for Congo red adsorption. *Separation and Purification Technology*, 260(2021), 1-43.
9. Nurdiana, A.; Astuti, L.; Dewi, R.P.; Ragadhita, R.; Nandiyanto, A.B.D; and Kurniawan, T. (2022). Techno-economic analysis on the production of zinc sulfide nanoparticles by microwave irradiation method. *ASEAN Journal of Science and Engineering*, 2(2), 143-156.
10. Nordin, N.A.H.M.; Ismail, A.F.; Racha, S.M.; Cheer, N.B.; Bilad, M.R.; Putra, Z.A.; and Wirzal, M.D.H. (2018). Limitation in fabricating PSf/ZIF-8 hollow fiber membrane for CO_2/CH_4 separation. *Indonesian Journal of Science and Technology*, 3(2), 138-149.
11. Astuti, L.; Dewi, R.P.; Nurdiana, A.; Ragadhita, R.; and Nandiyanto, A.B.D. (2021). Techno-economic analysis on the production of zinc sulfide nanoparticles by precipitation assisted ultrasonic radiation method. *International Journal of Research and Applied Technology* (*INJURATECH*), 1(1), 173-186.
12. Nandiyanto, A.B.D.; He, X; and W.-N. Wang. Colloid-assisted growth of metal–organic framework nanoparticles, *CrystEngComm*, 21(14), 2268-2272.
13. Nandiyanto, A.B.D. (2019) Nano metal-organic framework particles (i.e. MIL-100(Fe), HKUST-1(Cu), Cu-TPA, and MOF-5(Zn)) using a solvothermal process. *Indonesian Journal of Science and Technology*, 4(2), 220-228.
14. Ragadhita, R.; and Nandiyanto, A.B.D. (2020). Concentrations of metal ions and ligands on the formation of nano to submicron zinc imidazole framework-8 particles, *Journal of Engineering Science and Technology* (*JESTEC*), 15(1), 364-371.
15. Ragadhita, R.; and Nandiyanto, A.B.D. (2022). Curcumin adsorption on zinc imidazole framework-8 particles: isotherm adsorption using Langmuir,

Freundlich, Temkin, and Dubinin-Radushkevich models. *Journal of Engineering Science and Technology* (*JESTEC*), 17(2), 1078-1089.

16. Nandiyanto, A.B.D.; and Ragadhita R.: Feasibility study in the production of zinc imidazole framework particles. *Journal of Engineering Research*, 7(Special issue Oct 2019), 36-49.
17. Ragadhita, R.; and Nandiyanto, A.B.D. (2021). How to calculate adsorption isotherms of particles using two-parameter monolayer adsorption models and equations. *Indonesian Journal of Science and Technology*, 6(1), 205-234.
18. Abdelhamid, H.N. (2020). Hierarchical porous ZIF-8 for hydrogen production via the hydrolysis of sodium borohydride. *Dalton Transactions*, 49(14), 4416-4424.
19. Nandiyanto, A.B.D.; Hofifah, S.N.; Girsang, G.C.S.; Putri, S.R.; Budiman, B. A.; Triawan, F.; and Al-Obaidi, A.S.M. (2021). The effects of rice husk particles size as a reinforcement component on resin-based brake pad performance: From literature review on the use of agricultural waste as a reinforcement material, chemical polymerization reaction of epoxy resin, to experiments. *Automotive Experiences*, 4(2), 68-82.
20. Nandiyanto, A.B.D.; Ragadhita, R.; Fiandini, M.; Al Husaeni, D.F.; Al Husaeni, D.N.; and Fadhillah, F. (2022). Domestic waste (eggshells and banana peels particles) as sustainable and renewable resources for improving resin-based brakepad performance: Bibliometric literature review, techno-economic analysis, dual-sized reinforcing experiments, to comparison with commercial product. *Communications in Science and Technology*, 7(1), 50-61.
21. Nandiyanto, A.B.D.; Al Husaeni, D.N.; Ragadhita, R.; Fiandini, M.; Al Husaeni, D.F.; and Aziz, M. (2022). Resin matrix composition on the performance of brake pads made from durian seeds: From computational bibliometric literature analysis to experiment. *Automotive Experiences*, 5(3), 328-342.
22. Nandiyanto, A.B.D.; Putri, S.R.; and Kurniawan, T. (2022). Natural zeolite as the reinforcement for resin-based brake pad using dual particle size. *Journal of Engineering Science and Technology* (*JESTEC*), 17(4), 2512-2524.
23. Nandiyanto, A.B.D.; Hofifah, S.N.; Ragadhita, R.; Fiandini, M.; Al Husaeni, D.N.; and Maryanti, R. (2022). Resin-based brake pad with fleece fiber and its mechanical properties. *International Journal of Sustainable Transportation Technology*, 5(2), 51-54.
24. Anggraeni, S.; Anshar, A.N.; Maulana, A.; Nurazizah, S.; Nurjihan, Z.; Putri, S.R.; and Nandiyanto, A.B.D. (2022). Mechanical properties of sawdust and rice husk brake pads with variation of composition and particle size. *Journal of Engineering Science and Technology* (*JESTEC*), 17(4), 2390-2401.
25. Nandiyanto, A.B.N.; Husaeni, A.; Fitria, D.; Ragadhita, R.; Fiandini, M.; Rizky, K.M.; and Al Husaeni, D.N. (2022). The effect of mangosteen peel compositions as reinforcement components on resin-based brake pad performance with computational bibliometric mapping analysis. *Materials Physics and Mechanics*, 50(1), 37-55.
26. Nandiyanto, A.B.D.; Ragadhita, R.; Girsang, G.C.S.; Anggraeni, S.; Putri, S.R.; Sadiyyah, F.H.; and Hibatulloh, M.R. (2022). Effect of palm fronds and rice husk composition ratio on the mechanical properties of composite-based brake pad. *Moroccan Journal of Chemistry*, 10(4), 663-677.

27. Anggraeni, S.; Nandiyanto, A.B.D.; Ragadhita, R.; Girsang, G.C.S.; Putri, S.R.; Sadiyyah, F.H.; Rio, M.; Hibatulloh, V.; and Setiadi, D.P. (2022). Teaching the concept of brake pads based on composites of palm fronds and rice husks to high school students. *Journal of Engineering Science and Technology* (*JESTEC*), 17(5), 3149-3159.
28. Pratiwi, R.A.; and Nandiyanto, A.B.D. (2021). How to read and interpret UV-VIS spectrophotometric results in determining the structure of chemical compounds. *Indonesian Journal of Educational Research and Technology*, 2(1), 1-20.
29. Al-Ghouti, M.A.; and Da'ana, D.A. (2020). Guidelines for the use and interpretation of adsorption isotherm models: A review. *Journal of Hazardous Materials*, 393(2020), 1-22.
30. N'diaye, A.D. (2023). Nonlinear analysis of the kinetics and equilibrium for adsorptive removal of paranitrophenol by powdered activated carbon. *ASEAN Journal of Science and Engineering*, 3(3), 271-280.
31. Wang, Y.; Dai, X.; Zhan, Y.; Ding, X.; Wang, M.; and Wang, X. (2019). In situ growth of ZIF-8 nanoparticles on chitosan to form the hybrid nanocomposites for high-efficiency removal of Congo Red. *International Journal of Biological Macromolecules*, 137(2019), 77-86.
32. Khuluk, R.H.; and Rahmat, A. (2019). Removal of methylene blue by adsorption onto activated carbon from coconut shell (*Cocous nucifera L.*). *Indonesian Journal of Science and Technology*, 4(2), 229-240.
33. Nandiyanto, A.B.D.; Putri, S.R.; Anggraeni, S.; and Kurniwan, T. (2022). Isotherm adsorption of 3000-µm natural zeolite. *Journal of Engineering Science and Technology* (*JESTEC*), 17(4), 2447-2460.
34. Zulfiqar, M.; Lee, S.Y.; Mafize, A.A.; Kahar, N.A.M.A.; Johari, K.; and Rabat, N.E. (2020). Efficient removal of Pb (II) from aqueous solutions by using oil palm bio-waste/MWCNTs reinforced PVA hydrogel composites: kinetic, isotherm and thermodynamic modeling. *Polymers*, 12(2), 1-29.
35. Prihastuti, H.; and Kurniawan, T. (2022). Conversion of Indonesian coal fly ash into zeolites for ammonium adsorption. *ASEAN Journal for Science and Engineering in Materials*, 1(2), 75-84
36. Li, N.; Zhou, L.; Jin, X.; Owens, G.; and Chen, Z. (2019). Simultaneous removal of tetracycline and oxytetracycline antibiotics from wastewater using a ZIF-8 metal organic-framework. *Journal of Hazardous Materials*, 366(2019), 563-572.
37. Cho, H.S.; Yang, J.; Gong, X.; Zhang, Y.B.; Momma, K.; Weckhuysen, B.M.; and Terasaki, O. (2019). Isotherms of individual pores by gas adsorption crystallography. *Nature Chemistry*, 11(6), 562-570.
38. Tan, S.; Saito, K.; and Hearn, M.T. (2021). Isothermal modelling of protein adsorption to thermo-responsive polymer grafted sepharose fast flow sorbents. *Journal of Separation Science*, 44(9), 1884-1892.
39. Sa'adah, S.H. (2022). Effect of the mass of zeolite in curcumin solution on the adsorption process measured with luxmeter. *Molluca Journal of Chemistry Education* (*MJoCE*), 12(1), 8-22.
40. Hobday, C.L.; Woodall, C.H.; Lennox, M.J.; Frost, M.; Kamenev, K.; Düren, T.; and Moggach, S.A. (2018). Understanding the adsorption process in ZIF-8

using high pressure crystallography and computational modelling. *Nature Communications*, 9(1), 1-9.

41. Nandiyanto, A.B.D.; Putra, Z.A.; Andika, R.; Bilad, M.R.; Kurniawan, T.; Zulhijah, R.; and Hamidah, I. (2017). Porous activated carbon particles from rice straw waste and their adsorption properties. *Journal of Engineering Science and Technology* (*JESTEC*), 12(8), 1-11.
42. Ragadhita, R.; Nandiyanto, A.B.D.; Nugraha, W.C.; and Mudzakir, A. (2019). Adsorption isotherm of mesopore-free submicron silica particles from rice husk. *Journal of Engineering Science and Technology* (*JESTEC*), 14(4), 2052-2062.
43. Nandiyanto, A.B.D.; Hofifah, S.N.; Anggraeni, S.; and Kurniwan, T. (2022). Isotherm adsorption of 40-μm zeolite particles for treatment of dye wastewater. *Journal of Engineering Science and Technology* (*JESTEC*), 17(2), 1265-1275.
44. Nandiyanto, A.B.D.; Azizah, N.N.; and Taufik, R.S.R. (2022). Investigation of adsorption performance of calcium carbonate microparticles prepared from eggshells waste. *Journal of Engineering Science and Technology* (*JESTEC*), 17(3), 1934-1943.
45. Nandiyanto, A.B.D.; Hofifah, S.N.; and Maryanti, R. (2022). Identification of misconceptions in learning the concept of the adsorption process. *Journal of Engineering Science and Technology* (*JESTEC*), 17(2), 0964-0984.
46. Anggraeni, S.; Nandiyanto, A.B.D.; Pribadi, A.R.; Al-Kadzim, M.G.; Harefa, N.J.; Syabina, R.H.; and Girsang, G.C.S. (2022). The effect of rice husk composition on porous concrete performance. *Journal of Engineering Science and Technology* (*JESTEC*), 17(2), 1346-1355.